Insights into the Ethyl Lactate + Water Mixed Solvent

Santiago Aparicio* and Rafael Alcalde

Department of Chemistry, University of Burgos, 09001 Burgos, Spain

Received: May 19, 2009; Revised Manuscript Received: August 27, 2009

The mixed green solvent ethyl lactate + water is studied from macro- and microscopic viewpoints using a wide collection of experimental and computational tools. High-pressure thermophysical data, density, and dynamic viscosity provide valuable information on the macroscopic behavior of the mixed fluid, which is of remarkable importance for industrial purposes, and through the analysis of the derived excess and mixing properties lead to relationships with molecular level properties. Large deviations from ideality are obtained, which are related to the development of strong intermolecular hydrogen bonding between both molecules upon mixing. Computational studies, using the density functional theory, both in gas phase and water solution, allow to characterize, from energetic and structural viewpoints, the different ethyl lactate/water association complexes. The use of atoms in a molecule and natural bond orbital methods sheds light into the properties of ethyl lactate/water hydrogen bonding. Classical molecular dynamics simulations are carried out for the whole composition range, and as a function of pressure and temperature. Force field validation is done by comparison of predicted thermophysical properties with measured ones. Structural features are inferred from the analysis of radial distribution functions and their evolution with composition, pressure, and temperature, and dynamic aspects are inferred from the calculated self-diffusion constants and mean square displacements. The whole study points to a highly structured fluid, in which hydrogen bonding is developed both for water-rich and ethyl-lactate-rich solvents, showing a remarkable effect in the fluid structure upon the addition of the second component for both pure compounds, even more important for the effect of ethyl lactate on water hydrogen bonding network.

1. Introduction

The use of solvents is almost ubiquitous to all the chemical and related industries;[1,2] in fact, most of our understanding of chemistry has been developed in solution.[3−5] Solvents play a pivotal role in many processes such as chemical reactions, separation and product purification procedures, product carriers, washing and cleaning, and heat or mass transfer operations or even, because of their presence in many final products, directly used by the consumer. Moreover, they are used in a multiton scale and thus their production, handling, and use lead to remarkable environmental problems together with human or animal toxicological facts that should be considered with caution.[6] Many of the most widely used solvents may be classified as volatile organic compounds, and thus they are important atmospheric pollutants considering their known contribution to effects such as ozone depletion or global warming.[7] The increasing environmental regulations, arising from the social demand for cleaner and safer technologies and products, have strong consequences for the use of solvents in many different fields. Many of the organic solvents commonly used nowadays do not fulfill the principles of green chemistry[8] because they are volatile compounds and hazardous air pollutants, many of them are flammable fluids, and they are toxic for humans or surrounding environment. Hence, the use of these solvents leads to important environmental, health, and safety concerns, which are even more remarkable considering the large quantities of solvents used in the industry. Thus, alternatives to the use of traditional solvents have to be studied, and therefore, this is a subject of great interest both in industry and in academia.[6,9,10] The design of solvent-free processes or products is the most obvious alternative,[11] but although remarkable efforts have been done in this area, it is not feasible to eliminate the use of solvents for most of the operations in which they are involved, and thus new families of alternative solvents have to be explored. Nevertheless, the replacement of volatile organic solvents by new ones has to be done without stifling the technological development and at moderate economical costs, and new solvents should lead to the same, or even more, benefits than the traditional ones. There is no golden path for the substitution of traditional volatile organic solvents, and thus, different alternatives have to be studied carefully, considering that they should be compounds with low environmental impact, low toxicity both for humans and animals, readily biodegradable, easily recyclable, stable, with high solvency ability, readily available, and inexpensive. Two main alternative families of solvents have been considered by industry and academia: (i) supercritical fluids and (ii) ionic liquids.[1,12,13] These two alternatives are very promising, as the huge number of studies published in the literature show, but they have also some disadvantages, at least nowadays, over other possible fluids: (i) the use of many of them has important economical and technological costs when compared with traditional organic solvents, mainly for ionic liquid ones,[14] and (ii) their physical and chemical properties are still under academic study[15] and thus their industrial use is extremely rare.[16] Hence, other alternatives have to be considered, obviously without discarding any other one, that could replace in a direct way the traditional solvents.

Ethyl lactate, EL, is a very adequate alternative green solvent; it shows many environmental, toxicological, technological, and economical advantages for many applications.[17−20] It is 100% biodegradable, it does not show any potential health risk, it is

* Corresponding author. E-mail: sapar@ubu.es.

10.1021/jp904668e CCC: $40.75
Published on Web 10/05/2009

SCHEME 1

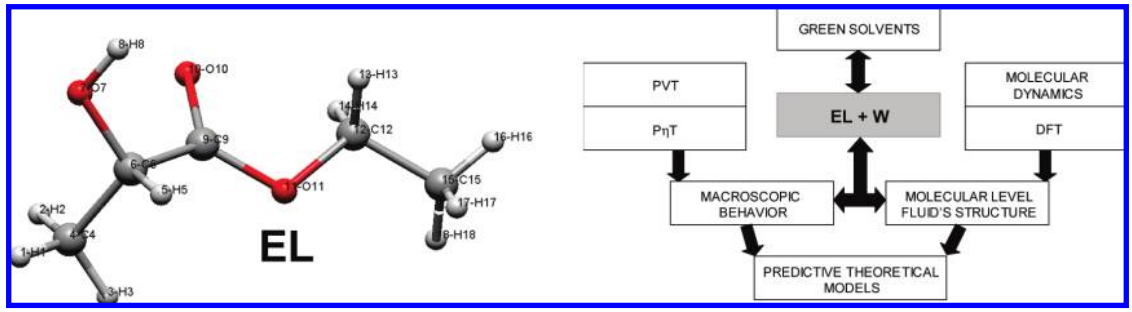

easy recyclable, noncorrosive, and non-ozone-depleting, and it has very suitable physical and chemical properties. It may be obtained from carbohydrate feedstocks at very low and competitive prices using recently developed technologies.[21−24] Moreover, the organic character of EL could lead to an easier replacement of traditional organic solvents considering that the industry would be less reluctant to its use. EL is produced from the esterification of lactic acid with ethanol using different procedures[23,25] leading to a mixed EL/water (W) product from which pure EL may be obtained. Thus, the knowledge of the properties of EL/W mixed solvent is of remarkable importance. As a continuation of our previous systematic studies[17,26] on EL-containing systems, we report here a wide combined experimental/computational study on the properties and structure of the EL/W mixed solvent. The use on a large scale of a new solvent, and thus the replacement of an existing one, requires, on one side, the accurate knowledge of their macroscopic properties in wide pressure and temperature ranges, and, on the other side, the understanding of the molecular level structure for the studied fluid and its relationship with macroscopic properties. This deep knowledge of the fluid behavior would allow to understand the processes developed in this solvent and to develop predictive tools for new processes and technologies. The methodology of the study reported in this work is explained in Scheme 1, together with the structure of EL molecule and the atom numbering used along this work. The main objectives of the work may be summarized as follows:

(i) To obtain accurate thermophysical data on EL + W binary system in the whole composition range, for wide pressure/temperature ranges. We have selected density (PVT behavior) and viscosity (PηT behavior) because of their importance for process design, and considering their intimate connection with molecular level features.

(ii) To obtain a detailed picture of the molecular level structure for this fluid, considering the effects rising from the competing development of hydrogen bonding between EL/W molecules (heteroassociation) and W/W and EL/EL molecules (homoassociation) together with the ability of EL to develop intramolecular hydrogen bonds. Thus, classical molecular dynamic simulations, MD, and quantum computations using density functional theory, DFT, were performed.

(iii) To relate the molecular level behavior with the macroscopic features of this mixed fluid, and thus, contribute to the development of structure−property relationships.

(iv) To provide with the required information for the use of this mixed fluid as an alternative green solvent to traditional organic ones.

2. Materials and Methods

The experimental and computational methodologies were reported previously in detail,[17] and thus we will describe them here only briefly.

Materials. EL ((−)-ethyl-(*S*)-2-hydroxypropionate, CAS No. 687-47-8), purchased from Fluka, 99.7% purity from gas chromatography, water content <0.05% from Karl Fischer coulometric titration, and ultrapure water (Milli-Q, Millipore, 18.2 mΩ·cm resistivity) were used for all the experiments. Mixture samples were prepared by weighing with a Metler AT261 balance ($\pm 1 \times 10^{-5}$ g), thus leading to $\pm 1 \times 10^{-4}$ accuracy for mole fraction.

PVT Behavior. The apparatus used in the PVT measurements was previously described in detail.[27] The system is installed around a high-pressure vibrating tube densimeter. The cell temperature was controlled and measured to $\pm 1 \times 10^{-2}$ K, and the pressure was kept constant to $\pm 5 \times 10^{-3}$ MPa and measured to $\pm 1 \times 10^{-2}$ MPa. The pressure transducer and thermometer were previously calibrated through well-defined and traceable procedures. For proper apparatus calibration, a 14-parameter equation was used[27] with *n*-hexane (Fluka, 99.9%) and water (Millipore, resistivity 18.2 mΩ·cm) as reference fluids.[28] The effect of samples' viscosity on density readings is below the accuracy limit of measurements ($\pm 1 \times 10^{-4}$ g cm^{-3}), and thus raw data without viscosity corrections were used in this work.

Experimental density data were fitted to the 10-parameter TRIDEN equation developed by Ihmehls and Gmehling.[29] From the fitting equation the derived properties isobaric thermal expansivity, α_P, isothermal compressibility, k_T, and internal pressure, P_i, were calculated.[30]

PηT Behavior. Viscosity measurements were carried out using an electromagnetic viscometer VINCI Tech. EV1000. Sample temperature was controlled with an external circulating bath and measured to $\pm 1 \times 10^{-2}$ K, and pressure was measured to $\pm 1 \times 10^{-2}$ MPa. Temperature and pressure sensors were previously calibrated through traceable procedures. Apparatus calibration was done using certified oils provided by the manufacturer. Viscosity accuracy was estimated to be $\pm 2\%$ in the full scale. Experimental viscosity data were fitted for the whole pressure−temperature range to a 7-parameter Tait-like equation.[31]

DFT Calculations. DFT calculations were carried out with the Gaussian 03 package[32] according to density functional theory (DFT), using the Becke gradient-corrected exchange functional[33] and Lee−Yang−Parr correlation functional[34] with the three-parameter (B3LYP)[35] method. 6-311++g** basis set was used in this work. Calculations in solution were carried out using the self-consistent reaction field approach (SCRF) with the solvent treated as a continuum using the integral equation formalism of the PCM approach (IEF-PCM).[36] The cavity in which the solute is placed in the IEF-PCM approach was built using the united atom model; in all the cases, a value of 1.2 was used to scale all the radii and 70 tesserae to divide the spherical surfaces. Atomic charges were calculated to fit the electrostatic potential[37] according to the Merz−Singh−Kollman (MK)[38] scheme. Interaction energies for complexes, ΔE, were

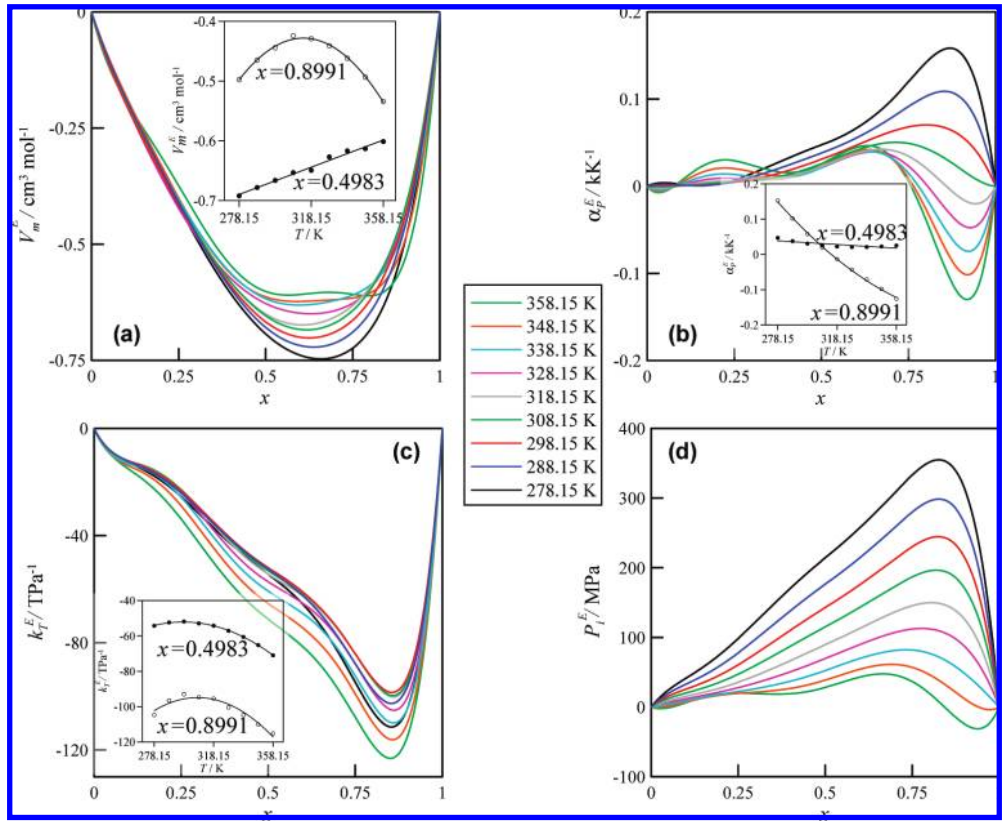

Figure 1. Effect of temperature on isobaric excess properties at $P = 30$ MPa for the x W + $(1 - x)$ EL mixed fluids. (a) Excess molar volume, V_m^E, (b) excess isobaric thermal expansivity, α_P^E, (c) excess isothermal compressibility, κ_T^E, and (d) excess internal pressure, P_i^E. x = water mole fraction. Lines show fitted data; symbols for experimental points are omitted for the sake of clarity.

calculated as the differences among the complex and sum of corresponding monomer energies at the same theoretical level, with basis set superposition error (BSSE) corrected through the counterpoise procedure.[39] Atoms in a molecule calculations[40] where carried out using the AIM2000 program.[41]

Molecular Dynamics Simulations. Classical molecular dynamics simulations were carried out using the TINKER molecular modeling package.[42] All simulations were performed in the NPT ensemble; the Nosé−Hoover method[43] was used to control the temperature and pressure of the simulation system. The motion equations were solved using the Verlet Leapfrog integration algorithm.[44] The molecular geometries were restrained according to SHAKE algorithm.[45] Long-range electrostatic interactions were treated with the smooth particle mesh Ewald method.[46] The simulated systems consist of cubic boxes with 200 total molecules to which periodic boundary conditions were applied in three directions. The simulations were performed using a cutoff $L/2$ Å radius for the nonbonded interactions, L being the box side. Initial boxes were generated using the PACKMOL program[47] to obtain adequate starting configurations. These boxes were minimized according to the MINIMIZE program in the TINKER package to a 0.01 kcal mol^{-1} Å^{-1} rms gradient; then several heating and quenching steps in the NVT ensemble up to 500 K were performed after which a 100 ps NVT equilibration molecular dynamics simulation was run at the set temperature; finally, from the output NVT simulation configuration, a run of 500 ps (time step 1 fs) in the NPT ensemble at the set temperature and pressure was run, from which the first 100 ps were used to ensure equilibration (checked through constant energy) and the remaining 400 ps for data collection. EL was described according to the optimized potential for liquid simulations (all-atom version) OPLS-AA,[48] with the parameters reported in a previous work,[17] whereas for water the SPC-E model was used.[49]

3. Results

Macroscopic Behavior. Thermophysical Properties. The macroscopic behavior of the studied mixed fluid is analyzed through the PVT and PηT properties measured in wide pressure−temperature ranges as a function of composition. Experimental density and viscosity data, together with fitting coefficients of correlation equations and calculated derived properties, are reported in Tables S1−S7 (Supporting Information). Composition, pressure, and temperature effects on the studied mixture properties are analyzed separately. Values for pure EL were reported in a previous work.[17] Excess properties were calculated according to previously reported ideality criteria,[27] and for viscosity, considering its nonthermodynamic character, a mixing function was defined according to the procedure previously reported.[50]

Excess molar volume, Figures 1a and 2a, is negative in the full composition range for all the studied pressures and temperatures. The EL/W mixture is a strongly nonideal system as it may be expected from the ability of the involved molecules to develop hydrogen bonds through homo- and heteroassociations. The mixing structure is additionally complicated because of the competing intra- and intermolecular hydrogen bonds in EL molecules.[17] Very effective packings are obtained upon mixing as the large negative excess molar volume shows. The arrangement of EL/W molecular level packings may originate from two main molecular factors: (i) steric effects, arising from the very different sizes and shapes of EL and W molecules and (ii) hydrogen bonding, because of the donor/acceptor hydrogen bonding ability of both molecules that should lead to different

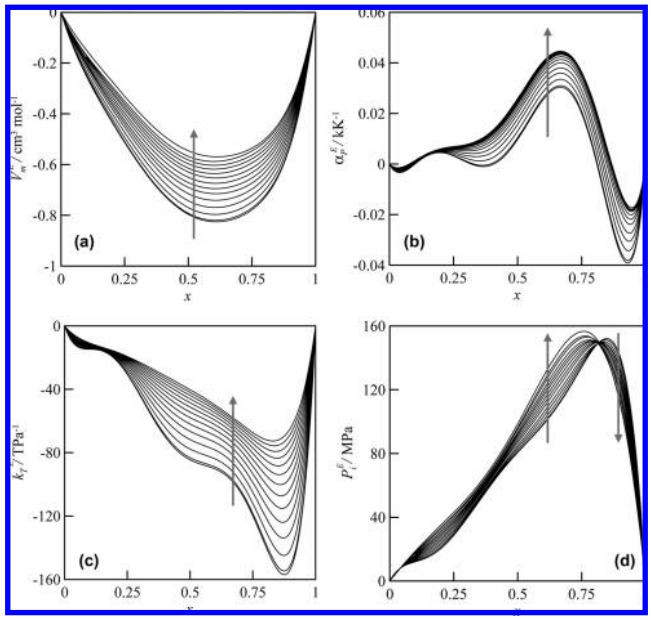

Figure 2. Effect of pressure on isothermal excess properties at $T = 318.15$ K for the x W + $(1 - x)$ EL mixed fluids. (a) Excess molar volume, V_m^E, (b) excess isobaric thermal expansivity, α_P^E, (c) excess isothermal compressibility, κ_T^E, and (d) excess internal pressure, P_i^E. x = water mole fraction. Arrows in the panels show increasing pressure from 0.1 to 60 MPa. Lines show fitted data; symbols for experimental points are omitted for the sake of clarity.

types of interactions upon mixing, together with the dynamics of these interactions. The minima of excess molar volume curves appear for 0.66 water mole fraction, which is in agreement with the density maxima for that mole fraction, and it is almost constant with pressure changes and moves toward lower water mole fractions with increasing temperatures (Figures 1a and 2a). Therefore, very efficient molecular packings are obtained for water-rich mixtures. Pure EL is slightly denser than pure water (3.1% at 298.15 K and 0.1 MPa),[26] but the free volume, V_F, in pure EL is remarkably larger than for pure water[17] (Figure 3). V_F is calculated for the studied mixtures from the fit of experimental PVT data to the Sanchez−Lacombe[51] equation of state using a procedure previously reported;[26] fitting parameters are reported in Table 1. As water mole fraction increases, the free volume decreases remarkably in an almost linear way, and the slope of V_F variation with temperature decreases too (Figure 3b). Hence, void space decreases as water mole fraction increases; this is in agreement with the well-known strong character and cooperativity of water hydrogen bonding, which is in contrast with the EL trend to form small aggregates, mainly dimers,[26] leading to larger void spaces. Calculated properties from PVT behavior, excess isobaric thermal expansivity, α_P^E, excess isothermal compressibility, κ_T^E, and excess internal pressure, P_i^E, show a complex behavior for temperature, pressure, and mixture composition variations. κ_T^E and P_i^E are negative and positive, respectively, for the studied pressure, temperature and composition ranges, whereas α_P^E shows close to zero values for $x_{water} < 0.5$ and values evolving from positive to negative with increasing temperature for $x_{water} > 0.5$. The global behavior of these properties may be explained considering that (i) water-rich EL/W mixtures lead to very efficient packings, and thus giving rise to density maxima, (ii) these packings produce poorly compressible fluids with low void spaces, and (iii) as the positive values of P_i^E show, these close packings allow very efficient intermolecular interactions between EL and W molecules. Therefore, EL seems to reinforce water hydrogen bonding through a very efficient interaction between both molecules. Nevertheless, although $P_i^E > 0$ values with maxima for water-rich regions point to very efficient intermolecular forces, it should be remarked that internal pressure only reflects partially hydrogen bonding between both molecules because of its own thermodynamic definition.[17,53]

To our knowledge, there is no experimental excess enthalpy data published in the literature for the ethyl lactate + water system, but published values for the closely related system methyl lactate + water[54] point to negative values, exothermic mixing, with minima for water-rich regions at water mole fractions close to those reported in this work for the studied properties reported in Figures 1 and 2. Therefore, we may infer exothermic mixing values for the ethyl lactate + water system, and thus, pointing again to the development of strong heteroassociation between EL and W molecules for water-rich mixtures. In this work, we report the pressure effect on excess enthalpy, excess entropy, and excess Gibbs energy calculated from PVT data, for the ethyl lactate + water system (Figure 4). As the pressure increases, a small endothermic contribution to excess enthalpy rises, and thus, hydrogen bonding is partially hindered at high pressures because of the disruptive effect of closer packings at high pressures. Nevertheless, considering the experimental large values of excess enthalpy for the methyl lactate + water system,[54] excess enthalpy for the ethyl lactate + water system should remain negative for the studied pressure range, at least for the lower temperatures. Moreover, as the pressure rises a positive excess entropic contribution appears with maxima for water-rich regions, and thus, for high pressures the disruptive effect of pressure on water hydrogen network is not fully balanced by the development of EL/W heteroassociations. The balance of enthalpic and entropic effects upon pressure increase leads to a negative contribution to excess Gibbs energy, and thus, to a prevailing entropic effect pointing to the disruption of water network with increasing pressure as the main molecular level factor. This would be in agreement with pressure effect on the remaining properties reported in Figure 2.

Viscosity and mixing viscosity are reported in Figure 5 as a function of pressure, temperature, and mixture composition. Dynamic viscosity shows a remarkably nonlinear behavior with mole fraction, showing maxima for water-rich mixtures ($x \sim 0.6$); these maxima decrease upon temperature increase and increase with increasing pressure, thus leading to very large positive mixing viscosity pointing to the development of heteroassociations that hinder the viscous flow.[55] The analysis of pressure and temperature effects on viscosity was carried out through the calculation of activation volume, $V^{\#}$, to analyze the pressure effect under isothermal conditions, and using the Arrhenius activation energy, E_a, to analyze the temperature effect for isobaric conditions, Figure 6. $V^{\#}$ was calculated using the equation reported in a previous work,[17] with successful fittings for the studied conditions. In a previous work, we reported that pure EL only showed Arrhenius-type behavior for $T > 298.15$ K, and this is also true for the studied EL + W mixtures. Thus, although fittings to more complex viscosity−temperature functions, such as Vogel−Fulcher−Tamman, lead to better results in the whole studied temperature range, we have fitted our data to a simple Arrhenius-type behavior, leading to satisfactory fits for $T > 298.15$ K, to obtain values of E_a as a function of water mole fraction for isobaric conditions. Moreover, the complex viscosity−temperature−pressure behavior of pure water is well-known,[56,57] and thus we understand that fitting the water viscosity data to the simple Arrhenius-type behavior fails to provide complete insights into the mechanism of water viscosity.

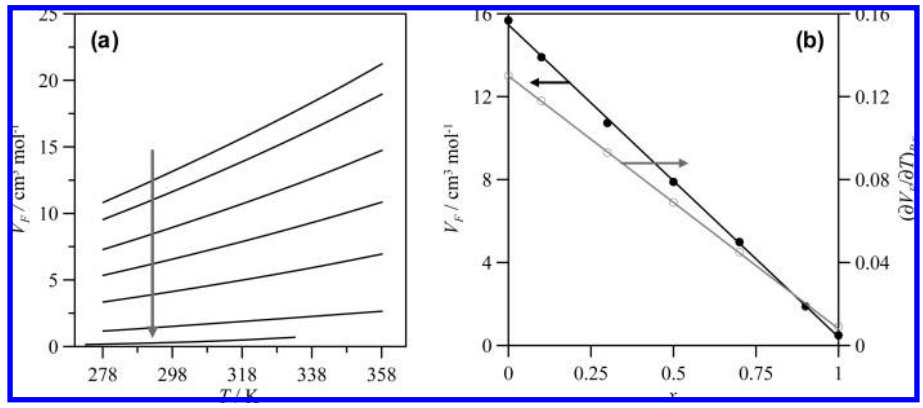

Figure 3. Free volume, V_F, estimated from Sanchez−Lacombe equation of state with parameters from Table 1 for the x W + (1 − x) EL mixed fluids. (a) Values for P = 0.1 MPa as a function of temperature for different mole fractions (from top to bottom, arrow indicates increasing temperature: x = 0, 0.0994, 0.3011, 0.4983, 0.7026, 0.8991, and 1). (b) Composition effect for P = 0.1 MPa and T = 318.15 K; the isobaric−isomolar slopes, $(\partial V_F/\partial T)_{P,x}$, are calculated considering linear trends in panel a. Lines in panel b are shown for guiding purposes. Values for pure water were obtained from ref 52.

TABLE 1: Parameters of Sanchez−Lacombe Equation of State Obtained by Fitting to Experimental PVT Data for the x W + (1 − x) EL Binary Mixtures[a]

x	P*/MPa[b]	r[b]	ε*/J mol^{-1}[b]	T*/K[c]	ρ*/kg m^{-3}[c]	υ*/cm^3 mol^{-1}[c]	hard-core volume (υ* × r)/cm^3 mol^{-1}[c]	%AAD
0 (pure EL)[d]	549.2	13.0	4295.3	516.6	1160.4	7.82	101.7	0.09
0.0994	548.9	11.8	4355.5	523.9	1159.0	7.94	93.3	0.09
0.3011	549.9	9.3	4505.0	541.9	1155.3	8.19	76.3	0.10
0.4983	600.2	7.6	4668.7	561.5	1152.6	7.78	59.1	0.10
0.7026	621.5	5.2	5056.5	608.2	1140.0	8.14	42.2	0.10
0.8991	565.0	2.2	6686.0	804.2	1091.5	11.83	25.7	0.17

[a] T*, P*, ρ* reducing characteristic parameters; r segment number of one molecule; ε* segment interaction energy; υ* segment volume; and %AAD percentage absolute average deviation of the fitting to experimental data. [b] Fitted parameters. [c] Calculated parameters. [d] Data from ref 26.

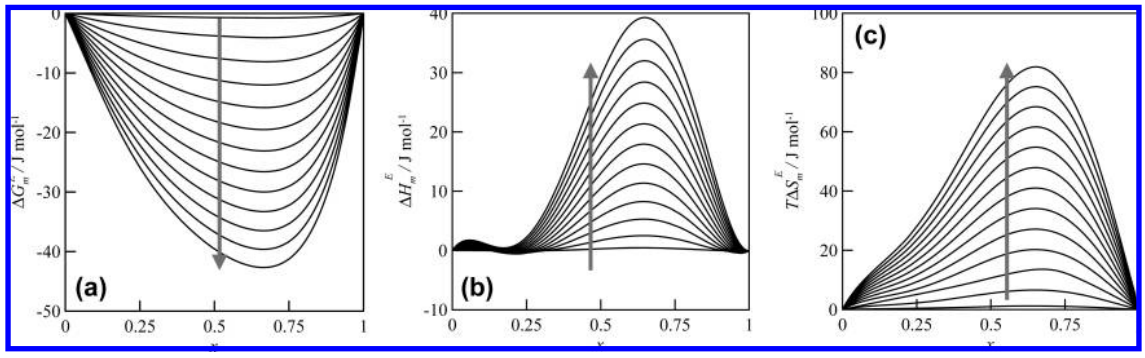

Figure 4. Pressure effect on the isothermal excess properties at T = 298.15 K with respect to their values at 0.1 MPa ($\Delta X = X_{298.15,P} - X_{298.15,0.1}$; where X stands for excess Gibbs energy, excess enthalpy or excess entropy) for the x W + (1 − x) EL mixed fluids. (a) Excess molar Gibbs energy, ΔG^E_m; (b) excess molar enthalpy, ΔH^E_m; (c) temperature and excess molar entropy factor, $T \cdot \Delta S^E_m$. x = water mole fraction. Arrows into the panels show increasing pressure from 0.1 to 60 MPa. Lines show fitted data; symbols for experimental points are omitted for the sake of clarity.

Nevertheless, considering that the purpose of this work is to study the behavior of EL/W mixtures, we have used the same approach to calculate viscosity derived properties from the reliable water viscosity data reported in the literature,[28] thus allowing a fair comparison that may lead to conclusions on EL/W mixture behavior. The pure water Arrhenius activation energy reported in Figure 6a is in good agreement with the available literature using a similar approach.[58,59] Once again, the behavior of both properties is remarkably different for water-rich zones with $x > 0.7$ and shows and almost linear variation with increasing EL concentration for $x < 0.7$; moreover, E_a and $V^{\#}$ for pure EL are larger than for pure W. Calculated viscosity activation energies may be considered as the sum of the energy necessary to create a hole within the fluid and the energy for a molecule to move toward that hole.[60,61] Hence, two main effects should control the viscosity behavior of the studied mixtures: (i) the molecular sizes and shapes that should contribute to increase viscosity for EL-rich mixtures compared with W-rich ones (larger holes should be created for the larger EL molecules), and (ii) the strength of intermolecular forces—the stronger the forces, the larger the viscosity and activation energies. The increasing values of E_a with the increasing W mole fraction show that the increasing water concentration leads to a very effective intermolecular interaction between EL and W molecules, and these complexes formed between both molecules through hydrogen bonding would require larger holes to allow viscous flow; considering that the available free volume reported in Figure 3 decreases as water mole fraction increases, this would lead to larger activation energies. A sudden change in both E_a and $V^{\#}$ appears for x in the 0.7−0.9 range, then, both properties decrease abruptly to the values of pure water, pointing to a weakening of intermolecular forces. Thus, strong intermo-

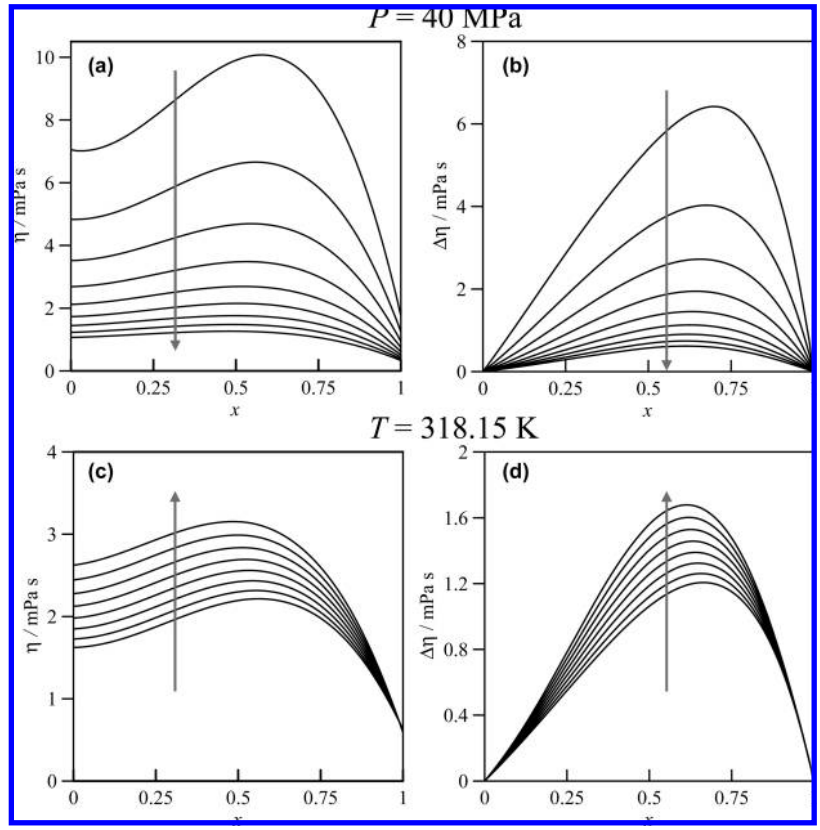

Figure 5. (a,b) Effect of temperature on isobaric viscosity and mixing viscosity at 40 MPa and (b,d) effect of pressure on isothermal viscosity and mixing viscosity at 318.15 K, for the x W + (1 − x) EL binary solvents. η = viscosity, and $\Delta\eta$ = mixing viscosity. x = water mole fraction. Arrows indicate increasing temperature from 278.15 to 358.15 K for panels (a) and (b) or increasing pressure from 1 to 70 MPa for panels (c) and (d). Lines show fitted data; symbols for experimental points are omitted for the sake of clarity.

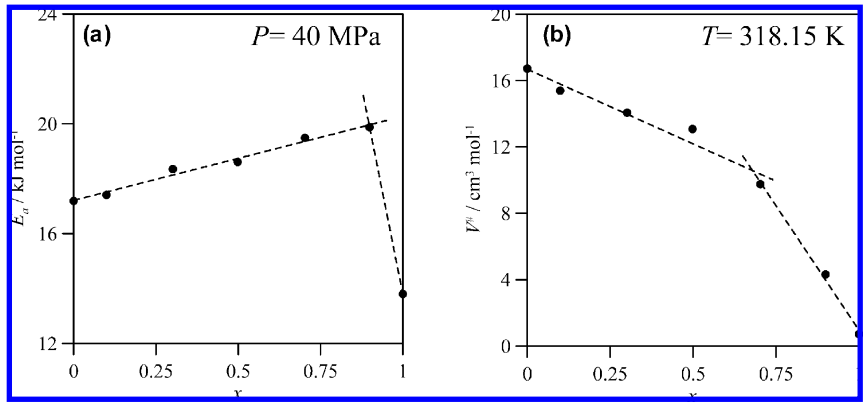

Figure 6. Activation volume, $V^{\#}$, and Arrhenius activation energy, E_a, for the x W + (1 − x) EL mixed fluids. Numerical values at the top of each panel report the (a) isobaric and (b) isothermal conditions for which both properties were calculated. Viscosity data used for calculation of activation properties reported in Table S6 (Supporting Information) are from ref 17 for pure EL and from ref 28 for pure W. E_a were calculated using viscosity data for T > 298.15 K to ensure Arrhenius-type behavior. $V^{\#}$ were calculated from equation reported in ref 17.

lecular forces are developed even for EL at high dilutions in water, and thus this molecule seems to reinforce the W hydrogen-bonding network as previous results pointed too.[26]

Microscopic Behavior from DFT Viewpoint. Although macroscopic thermophysical properties reported in the previous section provide some details on the microscopic behavior of the studied systems, because of the intimate connection between both approaches, this information is mostly of qualitative nature and should be handled with caution because the relationships between molecular level behavior and macroscopic information are neither simple nor direct. Therefore, molecular modeling may provide information on the molecular-level interactions that help to analyze the complex behavior of the studied mixtures. In this section, we will report the results of the DFT calculations carried out to obtain a better understanding of liquid-phase behavior for the studied systems, both in gas phase and in water solution. These results would allow inferring valuable information on the features rising from molecular sizes, shapes, and intermolecular forces that rule the behavior of these compounds, mainly for short-range interactions. Nevertheless, this should be taken with caution considering the additional complexity of liquid phases.

1 EL:1 W dimers, developed through hydrogen bonding, were studied both in gas phase and in water solution, using and IEF-PCM approach for water solution studies. EL molecules have four main positions through which they can interact with W

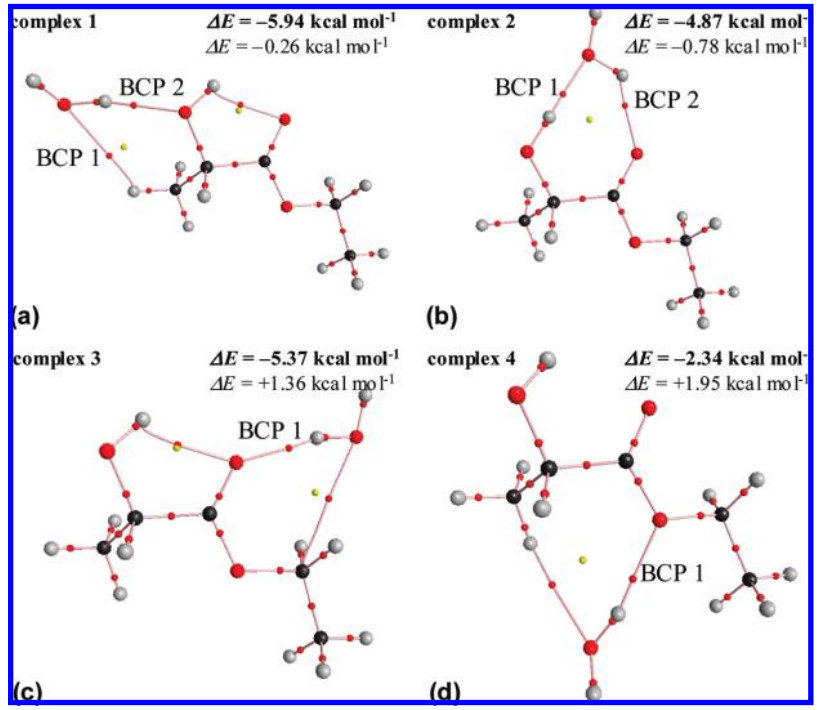

Figure 7. AIM analysis for 1 EL/1 W complexes computed in the gas phase at the B3LYP/6-311++G** theoretical level. Symbols: small red dots represent bond critical points, BCP; small yellow dots represent ring critical points, RCP; large dots represent attractors (atoms: black, carbon; red, oxygen; and gray, hydrogen) and pink lines represent bond paths. Ring paths are omitted for the sake of simplicity. ΔE = counterpoise-corrected binding energy in gas phase (bold) and IEF-PCM water.

TABLE 2: AIM Analysis of the Studied EL/W Complexes Computed in Gas Phase at the B3LYP/6-311++G Theoretical Level[a]**

complex	*BCP*	ρ_{BCP}/au	$\nabla^2\rho$/ au	*r*/Å	λ_1	λ_2	λ_3	ε	*G*	*H*	*V*	G/ρ_{BCP}
1	1	0.006	0.021	2.71	−0.0046	−0.0029	0.0284	0.5862	0.0044	0.0008	−0.0036	0.73
	2	0.030	0.113	1.88	−0.0459	−0.0432	0.2019	0.0625	0.0274	0.0007	−0.0267	0.91
2	1	0.032	0.125	1.82	−0.0520	−0.0482	0.2252	0.0788	0.0310	0.0003	−0.0307	0.97
	2	0.025	0.108	1.95	−0.0334	−0.0303	0.1712	0.1023	0.0239	0.0030	−0.0210	0.96
3	1	0.024	0.097	1.95	−0.0342	−0.0340	0.1649	0.0059	0.0221	0.0021	−0.0201	0.92
4	1	0.020	0.080	2.04	−0.0281	−0.0264	0.1349	0.0644	0.0181	0.0020	−0.0162	0.91

[a] Electron density at BCP, ρ_{BCP}; Laplacian of electron density at BCP, $\nabla^2\rho_{BCP}$; donor−acceptor interatomic distance, *r*; eigenvalues, λ_i, of Hessian of electron density; ellipticity, ε; kinetic energy density, *G*; potential energy density (or virial field), *V*; total energy density, *H*; and ratio between *G* and electron density at BCP, computed at the corresponding BCPs for each intermolecular hydrogen bonding. Values calculated for optimized structures reported in Figure 7.

molecules: (i) the hydroxyl oxygen, leading to open dimers (complex 1), (ii) the hydroxyl hydrogen and keto oxygen, leading to a cyclic dimer (complex 2), (iii) the keto oxygen, leading to an open dimer (complex 3), and (iv) the alkoxy oxygen (complex 4). Previous computational studies reported by our group[62] on the closely related methyl lactate + water interactions showed that the interaction through the alkoxy position is clearly hindered to develop hydrogen bonding with water molecules. This should be even more remarkable for EL molecules, in which the larger ethyl group would lead to and sterically hindered alkoxy group to develop interactions with water molecules. Thus, the counterpoise-corrected binding energies, ΔE, for the four proposed complexes, in both gas phase and IEF-PCM water solutions, are reported in Figure 7. Results show that interactions through 1−3 positions lead to similar interaction energies, with remarkable hydrogen bonding between both molecules but with a clear weakening of these interactions upon going to water solutions. Therefore, a highly dielectric media, as the one used for IEF-PCM calculations, seems to weaken EL/W hydrogen bonds; nevertheless, we should keep in mind that PCM approach considers the solvent as a continuum, and therefore this modeling fails to capture the subtle details rising from molecule to molecule interactions in liquid phases. The results point to almost equal probability of developing interactions through 1−3 positions, and discard the interactions through position 4.

Atoms in a molecule, AIM, analysis[40] of studied complexes will provide more detailed information on the characteristics of the intermolecular interactions. According to the AIM approach, two main criteria must be fulfilled to define a true hydrogen bonding:[63,64] (i) a bond path between two atoms, with the existence of a bond critical point, BCP, in the middle of the path and (ii) the electron density at BCP, ρ_{BCP}, and the Laplacian of that electron density, $\nabla^2\rho_{BCP}$, must be within the 0.002−0.035 and 0.024−0.139 ranges, respectively (both in atomic units); results are reported in Table 2 and Figure 7. We should remark that, according to the AIM theory, in the topology of electron density, there are some critical points, that is to say, the extrema of electron density where its gradient vector is null; if the critical point is placed between two nuclei, it is called BCP. Surprisingly, AIM method detects bond paths and BCP leading to cyclic dimers for the four studied complexes; nonetheless, an analysis of the ρ_{BCP} and $\nabla^2\rho_{BCP}$ properties discards the existence of H-bonding between water oxygen and

methyl hydrogens (Table 1). Only for complex 1 an interaction between the water oxygen and the methyl hydrogen leads to remarkable ρ_{BCP} and $\nabla^2\rho_{BCP}$ values, BCP 1 in Figure 7a; nevertheless, the ρ_{BCP} and $\nabla^2\rho_{BCP}$ values for this BCP are in the lower limit of the H-bonding range, and, moreover, the donor−acceptor interatomic distance is too large to define a truly hydrogen bond. The values of ρ_{BCP} and $\nabla^2\rho_{BCP}$ for the remaining interactions are large, with lower values for the BCP in complex 4, which is in agreement with the similar strength of complex 1−3 interactions, and the weaker character of complex 4, mainly because of the larger donor/acceptor distance for the alkoxy position interaction in complex 4, Table 1.

The energetic properties of BCP associated with hydrogen bonding also provide valuable information about these interactions according to the AIM approach. Kinetic energy density, G, is always positive, and its ratio to electron density, G/ρ_{BCP}, may be used to define the character of the interaction, considering that it used to be larger than 1.0 for closed shell (hydrogen bonding, ionic bonds, and van der Waals interactions) and less than 1.0 for shared interactions (covalent bonds).[40] Potential energy density (or virial field), V, that is always negative, is related to the covalency of the interaction[65] and with hydrogen-bonding strength through several empirical relationships.[66,67] It should be remarked that the relationship between V, G, and $\nabla^2\rho$ is through the local form of the virial theorem.[40] Moreover, total energy density, H, the sum of G and V, should be positive for closed-shell interactions, such as hydrogen bonding, indicating that kinetics energy density dominates the potential energy density, and negative for shared interactions.[40] The ratios G/ρ_{BCP} are slightly lower than 1.0 for all the studied complexes, although for closed-shell interactions as these ones they should be larger than 1.0;[40] nevertheless, values slightly lower than 1.0 have been previously reported for hydrogen bonding in other compounds.[65] H values are slightly positive for all the studied BCP, corresponding to strong hydrogen bonds. As a rule, the larger the G values, the stronger the hydrogen bonding and thus interactions in complexes 1−3 are stronger than in complex 4. Energetic properties for BCPs in complex 2 point to a slightly stronger interaction, although binding energies reported in Figure 7 are lower for this complex.

Natural bond orbital, NBO, analyses are reported in Table 3 and valuable information on the energy of studied hydrogen bonds may be inferred from them. Hydrogen bonding may be analyzed considering a charge transfer between the involved donor and acceptor atoms. Thus, hydrogen bonding rising from EL hydroxyl oxygen (complex 1), keto oxygen (complex 2 and 3), and alkoxy oxygen (complex 4) toward W OH groups, and from water oxygen toward EL hydroxyl hydrogen (complex 2), should be determined by the hyperconjugation-induced charge transfer between the corresponding oxygen electron lonely pairs (donor) and the antibonding orbitals for the hydroxyl bond (acceptor), $n_O \rightarrow \sigma^*_{O-H}$ (Table 3). Three main properties are considered to analyze hydrogen bonding in the studied complexes according to the NBO approach: (i) second-order perturbation energy, $E(2)$, (ii) energy difference among the donor and the acceptor, ΔE, and (iii) Fock matrix element between the donor and acceptor, F_{ij}, that reflects the symmetry between donor and acceptor orbitals. Therefore, the larger the $E(2)$, the stronger the hydrogen bonding. Moreover, $E(2)$ may increase because of the low values of ΔE, and/or the large F_{ij} values, that show good symmetry between donor and acceptor orbitals, thus improving the donor/acceptor charge transfer and leading to a stronger hydrogen bonding. All the studied hydrogen bonds show poor symmetry between donor and acceptor orbital, as the low F_{ij} values show, and the only exception is the transference from the W lonely pair toward the EL hydroxyl group, which shows the larger $E(2)$ values. The studied interactions show almost equal properties for the interactions from both oxygen lonely pairs, because for pairs of type 1 ΔE is larger but symmetry is better than for pairs of type 2. Thus, both oxygen lonely pairs seem to contribute in an almost equal fashion to the studied hydrogen bonds. Only for complex 4, the interaction is carried out though a single lonely pair because pair 2 is sterically hindered, and this fact would justify the weaker character of hydrogen bonding for this complex.

TABLE 3: NBO Analysis of the Studied EL/W Complexes Computed in Gas Phase at the B3LYP/6-311++G Theoretical Level[a]**

complex	donor	donor pair	acceptor	$E(2)$/kcal mol^{-1}	ΔE/au	F_{ij}/au
1	O7	1	HO in W	3.52	1.03	0.054
		2		5.53	0.84	0.061
2	O in W	1	H8 - O7	–	–	–
		2		11.27	1.08	0.099
	O10	1	HO in W	2.12	1.16	0.045
		2		1.90	0.74	0.035
3	O10	1	HO in W	2.83	1.19	0.052
		2		3.31	0.76	0.046
4	O11	1	HO in W	3.27	1.04	0.052
		2		–	–	–

[a] Second-order perturbation energy, $E(2)$, energy difference among the donor and the acceptor, ΔE, and Fock matrix element between the donor and the acceptor, F_{ij}. Values calculated for optimized structures reported in Figure 7. Reported values only for $E(2) > 0.50$ kcal mol^{-1}. Hyperconjugation-induced charge transfers are of $n_O \rightarrow \sigma^*_{O-H}$ type, from the oxygen lonely pairs (pair 1 or 2) to the corresponding antibonding O−H orbital, with the donor pairs belonging to EL (O7, O10, or O11) and the acceptor belonging to water, except for the first interaction in complex 2 in which the donor belongs to W and the acceptor to EL. Atom numbering as in Scheme 1.

TABLE 4: Free Energy of Solvation, ΔG_{sol}, and Electrostatic, ΔG_{elec}, and Nonelectrostatic, $\Delta G_{nonelec}$, Contributions to ΔG_{sol}, of the Studied EL/W Complexes Computed in IEF-PCM Water Solution at the B3LYP/6-311++G Theoretical Level[a]**

complex	ΔG_{sol}/kcal mol^{-1}	ΔG_{elec}/kcal mol^{-1}	$\Delta G_{nonelec}$/kcal mol^{-1}
1	−2.55	−14.10	11.55
2	−3.61	−14.96	11.35
3	−1.51	−13.97	12.46
4	−1.13	−13.07	13.15

[a] Values calculated for optimized structures reported in Figure 7.

Finally, solvation properties of the studied complexes on IEF-PCM water media are reported in Table 4. Free energies of solvation show moderate values because of the large positive nonelectrostatic positive contributions rising from the large cavitation energies (∼25−26 kcal mol^{-1}, for the four studied complexes). This behavior would justify the weakening of hydrogen bonding upon going to a high dielectric media as IEF-PCM water. Moreover, although the values of calculated dipolar moments for the studied complexes (∼ 4 D) would lead to a remarkable interaction with the reaction field, as the large negative electrostatic contributions show, Table 4, the work required to build the cavities for the large complexes would be the prevailing factor in the solvation energies.

Microscopic Behavior from Molecular Dynamics Simulations. Classical molecular dynamics (MD) simulations allow to obtain a more detailed picture of the microscopic structure

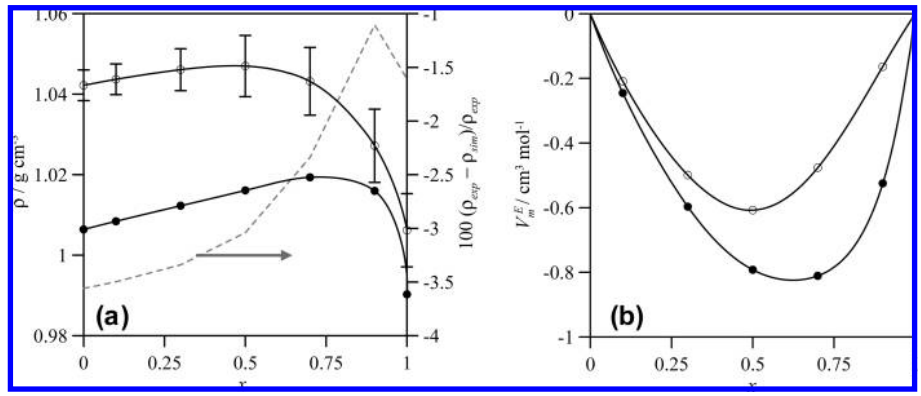

Figure 8. Comparison between experimental and calculated, from molecular dynamics simulations, properties for the x W + (1 − x) EL mixed fluids at 318 K and 0.1 MPa. x = water mole fraction; ρ = density, and V_m^E = excess molar volume. (●) Experimental and (○) calculated properties; continuous lines showed for guiding purposes.

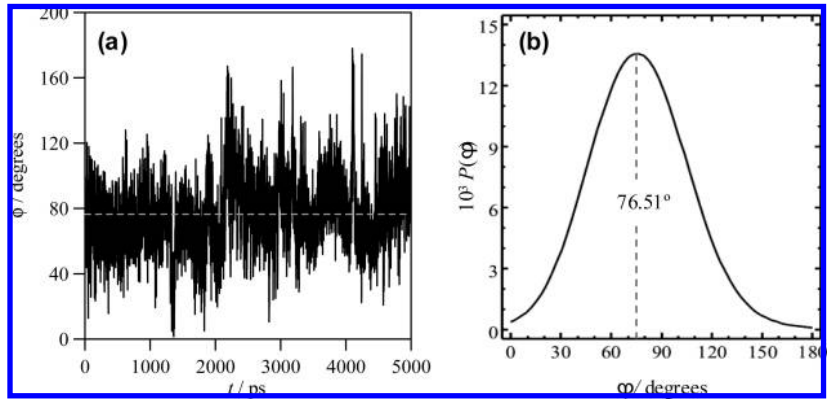

Figure 9. (a) Time evolution and (b) distribution function for 7−6−9−10 dihedral angle in EL, atom numbering as in Scheme 1, for x W + (1 − x) EL mixed fluids at 318 K and 0.1 MPa with x = 0.3. x = water mole fraction. Values obtained from molecular dynamics simulations. Dashed line in panel (a) shows the maxima of distribution function reported in panel (b).

for the studied mixed fluids, considering medium- and large-range effects that were lost in the short-range DFT computational studies reported in the previous section. MD simulations were performed for 0, 0.1, 0.3, 0.5, 0.7, and 0.9 water mole fractions at 278, 318, and 358 K and 0.1, 30, and 60 MPa, to analyze composition, pressure, and temperature effects on structural features. Simulations for pure EL were reported in a previous work.[17]

Although EL force field parametrization validation was performed in a previous work,[17] and the strengths and weaknesses of SPC-E model for pure water are well-known, we have studied the ability of both models to describe the macroscopic behavior of the studied mixed fluids, and thus density comparisons were performed. We report in Figure 8 comparisons between experimental and calculated density as a function of water mole fraction at 318 K and 0.1 MPa. Predicted densities are always larger than experimental ones, with deviations around −3% for $x < 0.5$ and decreasing to −1.5% as we approach to pure water. Excess molar volume is underestimated by MD simulations, because of the larger densities predicted for pure EL. Nevertheless, the shapes and trends of density and excess molar volume curves are predicted accurately by the proposed force field parametrization, and thus, although the model slightly overestimates intermolecular interactions in pure EL, probably because of the use of MK charges for EL simulations that lead to stronger Coulombic forces,[17] most of the structural features in the studied mixed fluids are captured successfully by the proposed force field parametrization. Similar quality of properties prediction is produced in the remaining pressure/temperature ranges studied.

An important question to analyze the structure of EL/W mixtures is the preferred conformation of EL molecules in water solutions, because of the competing effects of intramolecular hydrogen bonding between the hydroxyl and keto groups within EL molecules, with the surrounding EL and W molecules. In a previous work,[17] we reported that the EL hydroxyl group is clear out-of-plane skewed in pure EL fluids, and thus intramolecular hydrogen bonding is hindered to favor EL/EL heteroassociations. Results reported in Figure 9 for 7−6−9−10 dihedral angle (atom code, Scheme 1), which show the relative position of hydroxyl and keto groups in EL molecule, point to a slightly larger dihedral angle than in pure EL (73° in pure EL and ∼77° for all the studied EL/W mixtures), and thus, intramolecular EL hydrogen bonding in EL molecules should be discarded for EL/W mixtures.

The analysis of MD-calculated intermolecular interaction energies, E_{inter}, is important because it provides information on the evolution of intermolecular forces upon changing composition for mixed fluids. Results reported in Figure 10 lead to several conclusions. First, E_{inter} for pure EL is larger than for pure W, because of the larger enthalpy of vaporization for liquid EL (52.5 and 43.99 kJ mol^{-1} for EL and W, respectively, both at 298.15 K and normal pressure).[68,69] Second, E_{inter} decreases in a linear fashion up to $x = 0.9$ and then it decreases in a steeped way to the values of pure water. Therefore, EL molecules have a strong effect on W hydrogen-bonding structure, reinforcing it and leading to larger E_{inter} values. This behavior is in agreement with the conclusions derived from macroscopic thermophysical properties, especially with the viscosity activation energy reported in Figure 6a.

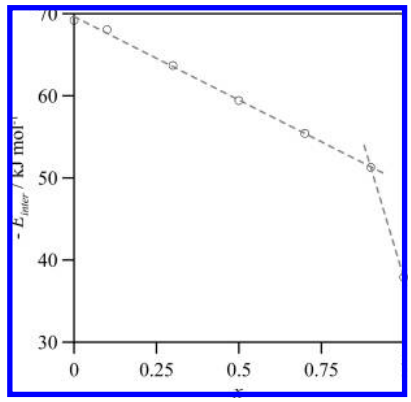

Figure 10. Intermolecular interaction energy, E_{inter}, for the x W + (1 − x) EL mixed fluids, calculated from molecular dynamics simulations at different concentrations at 318 K and 0.1 MPa. x = water mole fraction. (○) Calculated values. Dashed lines show linear fits for $x < 0.9$ and for $x > 0.9$.

Structural molecular level features are analyzed in a first approach using radial distribution functions, RDFs, which are reported for selected pairs in Figure 11 as a function of mixture composition for isobaric/isothermal conditions. Homoassociations in mixture are studied through the 8−10 (hydroxyl hydrogen−carbonyl oxygen), 8−7 (hydroxyl hydrogen-hydroxyl oxygen) and 15−15 (carbon in ethyl group) pairs for EL, and through Ow-Hw pair for water, whereas heteroassociations are analyzed using the 8-Ow and 10−Ow pairs. RDFs for 8−10 pair shows a narrow and strong peak with maxima at 1.95 Å, although the intensity of the peak decreases with increasing water mole fraction, the position of the maxima do not change. RDFs for 8−7 show maxima at the same distance than 8−10, but the intensity of the peaks is remarkably lower, and thus 8−10 interactions would be preferred over 8−7 ones. In a previous work,[17] we showed that this behavior points to a remarkable population of cyclic EL dimers, which would prevail even for EL diluted in W solutions. The interaction between EL apolar groups, 15−15 RDFs, shows two maxima for 4.10 and 8.25 Å, which do not change either their position or intensity with increasing EL dilution in W. Therefore, interactions between EL molecules is not affected remarkably by the presence of water molecules, EL molecules tend to self-aggregate in a similar way to pure EL. The interaction between water molecules from the Ow−Hw RDFs show the two characteristic peaks at 1.80 and 3.25 Å. The positions of the maxima for these peaks do not change with increasing EL mole fraction, and their amplitudes are higher with increasing EL mole fraction, which point to an enhancing effect of EL on water structuring. Therefore, it may be concluded that EL interactions do not change remarkably with water dilution and W structure is clearly reinforced by the presence of EL molecules. The next question is how both molecules interact between them. The energy of EL dimers (−5. 49 kcal mol^{-1} in gas phase, for cyclic dimers)[17] is similar to that for 1 EL:1 W complexes reported in Figure 7, and thus homo and hetero hydrogen bondings should compete upon EL/W mixing. Results reported in Figure 11, e and f, for 8-Ow (EL hydroxyl/W interaction) and 10-Hw (EL keto and W interaction) show remarkable hydrogen bonding between both molecules, because of the sharp peaks with maxima at 1.95 and 3.35 Å for 8-Ow and 1.75 and 3.15 Å for 10-Hw pairs. The interatomic distances for these maxima are in good agreement with gas-phase DFT results reported in Table 2 and Figure 7, thus showing that DFT calculations provide a good representation of short-range hydrogen bonding in the studied mixed fluids. The amplitude of 8-Ow peak is larger than that of 10-Hw for low water mole fractions, but as W concentration increases, 10-Hw amplitude is larger, and thus, interaction through EL hydroxyl position is preferred for low W concentrations, whereas for larger W mole fractions EL keto position is preferred. Nonetheless, interactions through both positions are developed in the whole concentration range. It should be remarked that there is similarity between the 8-Hw peak and the Ow-Hw peak, pointing to the replacement of some water by EL molecules in the water hydrogen bonding network.

To analyze the existence of microheterogeneities in the studied mixed fluids, we have calculated the water local mole fraction around EL molecules. We have considered the local composition within a sphere, centered in EL hydroxyl hydrogen (because of the sharp peaks for the water interaction through this site reported in Figure 11), with a radius of 3.95 Å, which is the position of the minima after the second sharp peak of 8-Ow RDFs reported in Figure 11e. Thus, the two solvation spheres around EL molecules, which may be inferred from the analysis of RDFs reported in Figure 11, are included. The number of water molecules around EL ($n_{H8,OW}$, using H8 atom as a representative of EL molecule, and Ow for W molecule) was calculated according to eq 1:

$$n_{H8,ow} = \rho_{ow} \int_0^{3.95} g_{H8-ow} 4\pi r^2 \, dr \qquad (1)$$

where ρ_{OW} is the bulk number density and $g_{H8\text{-}OW}$ is the RDF for the 8-Ow pair. Thus, water local mole fraction, x_{local}, is defined using eq 2, and reported in Figure 12 in comparison with bulk water mole fraction.

$$x_{H8,ow} = \frac{n_{H8,ow}}{n_{H8,ow} + n_{H8,H8}} \qquad (2)$$

x_{local} is remarkably different from bulk water mole fraction, being larger for $x < 0.7$ and lower for $x > 0.7$. Thus, water molecules tend to clusterize around water molecules when EL concentration is large, whereas for large water mole fraction the reinforcement of water hydrogen bonding network mentioned in the previous paragraph leads to a slightly decrease of water molecules in the EL solvation spheres. Nevertheless, the clustering of W molecules around EL molecules for $x < 0.7$ is more remarkable than the lower local mole fraction in comparison with bulk ones for large water mole fraction; for example, at $x = 0.5$, $x_{local} = 0.63$ (a 26% larger local water concentration), whereas for $x = 0.9$, $x_{local} = 0.85$ (just a 5.6% lower local mole fraction).

The number of hydrogen bonds per molecule, n_{HB}, is another important information that may be extracted from the analysis of RDFs. RDFs reported in Figure 11 show that we have three well-defined types of interactions through hydrogen bonding: EL/EL, W/W, and EL/W complexes. We define each occurrence within 2.85 Å for EL/EL H-bonds (the first minima in Figure 11a, the radii of the first coordination shells), within 2.45 Å for W/W H-bonds (Figure 11d) and within 2.55 Å for EL/W H-bonds (Figure 11, e and f). No remarkable effect of considered angles, within reasonable values, was found on the extension of hydrogen bonding, and thus, a 60° value was used for all the possible interactions. Results of hydrogen-bonding extension using this simple hydrogen-bonding criteria are reported in Figure 13. Results for pure water at 318 K/0.1 MPa show 3.3 hydrogen bonds per water molecule, which is in fair agreement

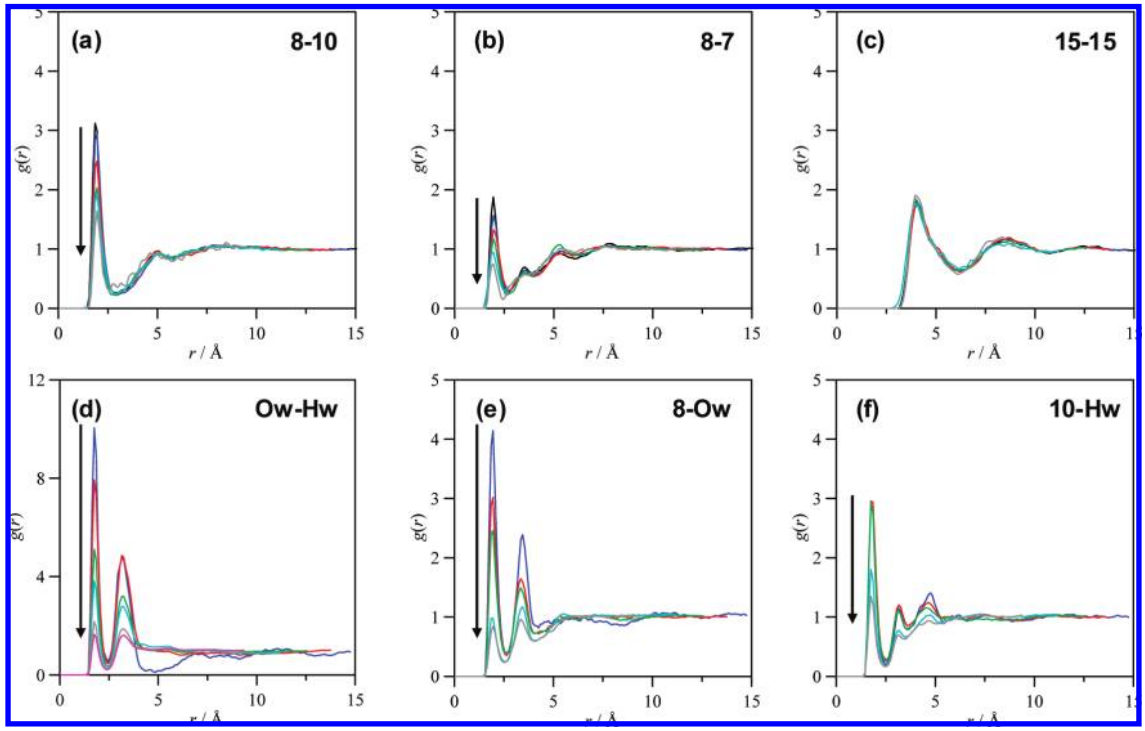

Figure 11. Site−site radial distribution functions, $g(r)$, for the x W + $(1 - x)$ EL mixed fluids, calculated from molecular dynamics simulations at different concentrations at 318 K and 0.1 MPa. x = water mole fraction. Arrows indicate increasing water mole fraction. (black) $x = 0$ (pure EL), (blue) $x = 0.1$, (red) $x = 0.3$, (green) $x = 0.5$, (cyan) $x = 0.7$, (gray) $x = 0.9$ and (pink) $x = 1$ (pure W). Atom numbering as in Scheme 1.

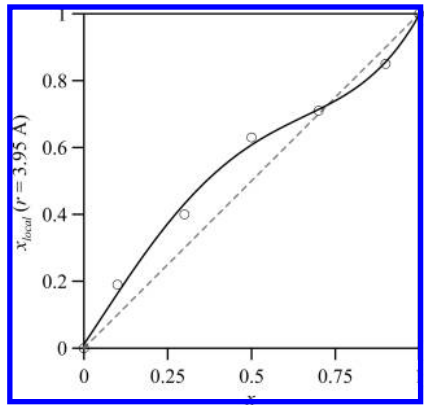

Figure 12. Local mole fraction of water, x_{local}, around EL, within a sphere of radius $r = 3.95$ Å centered in H8 atom of EL, for the x W + $(1 - x)$ EL mixed fluids, calculated from molecular dynamics simulations at different concentrations at 318 K and 0.1 MPa. Continuous line shown for guiding purposes and dashed line to indicate when local mole fraction is equal to bulk mole fraction. x = bulk water mole fraction.

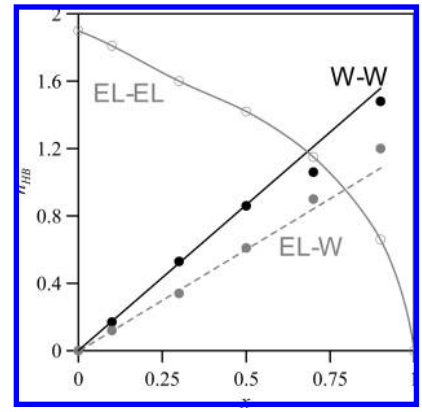

Figure 13. Number of hydrogen bonds, n_{HB}, between EL molecules, EL−EL, per EL molecule, between W−W molecules, per W molecule, and between EL−W molecules, per EL molecule, for the x W + $(1 - x)$ EL mixed fluids, calculated from molecular dynamics simulations at different concentrations at 318 K and 0.1 MPa. x = water mole fraction.

with literature results.[70] For pure EL, two hydrogen bonds are developed in the whole composition range, which are divided in EL/EL and EL/W interactions. EL/EL number of interactions show a remarkably different behavior, with a clear nonlinear variation with water mole fraction, in comparison with EL/W and W/W ones, for which a linear increase with water mole fraction is obtained. Thus, the main effect on these mixtures rises from the remarkable trend of EL molecules to self-aggregate though hydrogen bonding, which lead to a very rapidly increase of EL/EL H-bonds with increasing EL mole fraction; for example, for 0.7 water mole fraction, the EL−EL number of hydrogen bonds per molecule is 59% of that in pure EL. Nevertheless, at large water mole fraction, EL molecules interact very efficiently with W molecules, leading at the same time to a reinforcing of W/W interactions. Thus, this delicate balance between the trend of EL molecules to self-associate and their effective interaction with W molecules should determine EL/W molecular level structure. The behavior of EL/EL number of hydrogen bonds resembles those of thermophysical properties reported in Figures 1−5, and it would justify that excess and mixing properties would show maxima/minima around 0.7 water mole fraction. Moreover, we may expect that, for systems for which the trend to self-aggregate of lactate molecules is not balanced by remarkable interactions with water molecules, we may have immiscibility regions. Our first unpublished results for isopropyl and butyl lactate + water mixtures confirm that these systems are immiscible for lactate-rich regions because of the large hydrophobic alkylic groups hindering the development of H-bonding with water molecules.

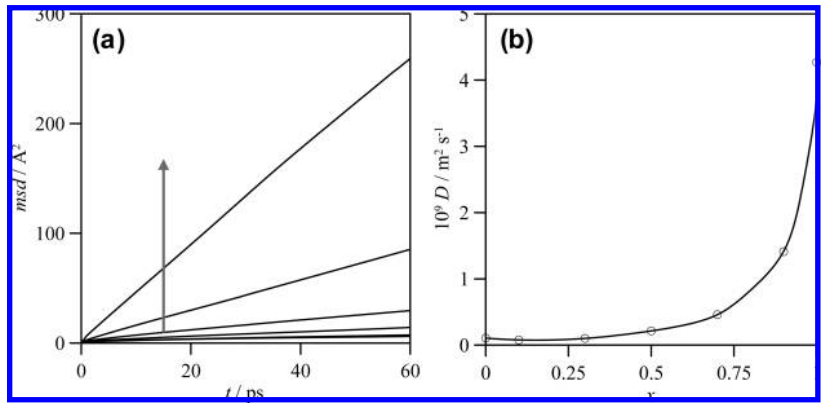

Figure 14. Mean square displacement, msd, and diffusion coefficient, D, for the x W + (1 − x) EL mixed fluids, calculated from molecular dynamics simulations at different concentrations at 318 K and 0.1 MPa. x = water mole fraction. In panel (a) arrow indicate increasing water mole fraction, from bottom to top $x = 0.0$ (pure EL), 0.1, 0.3, 0.5, 0.7, 0.9, and 1.0 (pure water).

Dynamic properties are important quantities, not easily measurable, to characterize fluids. The self-diffusion coefficient, D, may be calculated from Einstein's relation:

$$D = \frac{1}{6}\lim_{t\to\infty}\langle \Delta r(t)^2 \rangle \qquad (3)$$

where the quantity in broken brackets, the mean square displacement msd, is plotted in Figure 14, as a function of composition, together with the D values calculated from the slopes of linear fittings of msd. Self-diffusion coefficient for pure EL is remarkably lower than for pure W, on one side because of the strong intermolecular interactions in pure EL, and on the other side because of the larger size of EL molecules. For the EL/W mixtures, two regions are inferred from the D variation with water mole fraction: for $x < 0.7$, a very small, almost linear increase with water mole fraction is obtained, whereas for $x > 0.7$ a steeped increase of D is obtained. Thus, remarkable W/EL interactions lead to the decrease of mixture self-diffusion coefficient, even for highly diluted solutions; for example, for $x = 0.9$, self-diffusion coefficient decreases 66% compared with the value for pure SPC-E water. This is in agreement with the reinforcing ability of EL molecules on W hydrogen bonding network, inferred from the whole theoretical/experimental properties reported in the previous sections.

4. Conclusions

The main conclusions of the combined experimental/theoretical study of EL/W mixed fluids reported in this work are as follows:

(i) Strongly nonideal behavior is obtained, because of the complex hydrogen-bonding interactions in the mixtures, with maxima/minima of excess and mixing properties around 0.7 water mole fraction.

(ii) Very efficient W/EL interactions through hydrogen bonding, more remarkably for low EL concentrations.

(iii) Strong trend of EL molecules to self-associate in water mixtures, even for diluted solutions, that should lead to immiscibility regions for higher members of the lactate family.

(iv) The balance of EL/EL and EL/W interactions determine the mixed fluids structure, prevailing EL/EL hydrogen bonds for $x < 0.5$.

(v) Reinforcement of W hydrogen bonding network for low EL mole fractions with a strong effect of EL molecules on mixtures' properties.

Supporting Information Available: Density (Table S1), TRIDEN fitting coefficients of density (Table S2), isobaric expansibility (Table S3), isothermal compressibility (Table S4), internal pressure (Table S5), dynamic viscosity (Table S6), and fitting coefficients of dynamic viscosity (Table S7). This material is available free of charge via the Internet at http://pubs.acs.org.

References and Notes

(1) DeSimone, J. M. *Science* **2002**, *297*, 799.
(2) Archer, W. L. *Industrial Solvents Handbook*; Marcel Dekker: New York, 1996.
(3) Reichardt, C. *Solvents and Solvent Effects in Organic Chemistry*; Wiley-VCH: Weinheim, Germany, 2003.
(4) Marcus, Y. *The Properties of Solvents*; Wiley: Chichester, UK, 1998.
(5) Buncel, E.; Stairs, R. A.; Wilson, H. *The Role of Solvents in Chemical Reactions*; Oxford University Press: Oxford, UK, 2003.
(6) Capello, C.; Fischer, U.; Hungerbühler, K. *Green Chem.* **2007**, *9*, 927.
(7) Allen, D. T.; Shonnard, D. R. *Green Engineering*; Prentice Hall: Upper Saddle River, NJ, 2002.
(8) Anastas, P. T.; Warner, J. C. *Green Chemistry: Theory & Practice*; Oxford University Press: Oxford, UK, 1998.
(9) Sheldon, R. A. *Green Chem.* **2005**, *7*, 267.
(10) Nelson, W. N. *Green solvents for chemistry: perspectives and practice*; Oxford University Press: New York, 2003.
(11) Metzger, J. O. *Angew. Chem., Int. Ed.* **1998**, *37*, 2975.
(12) Plechkova, N. V.; Seddon, K. R. *Chem. Soc. Rev.* **2008**, *37*, 123.
(13) DeSimone, J. M., Tumas, W., Eds.; *Green Chemistry using liquid and supercritical carbon dioxide*; Oxford University Press: New York, 2003.
(14) Kralisch, D.; Stark, A.; Körsten, S.; Kreisel, G.; Ondruschka, B. *Green Chem.* **2005**, *7*, 301.
(15) Marsh, K. N.; Boxall, J. A.; Lichtenthaler, R. *Fluid Phase Equilib.* **2004**, *219*, 93.
(16) Short, P. L. *Chem. Eng. News* **2006**, *84*, 15.
(17) Aparicio, S.; Alcalde, R. *Green Chem.* **2009**, *11*, 65.
(18) Warner, J. C.; Cannon, A. S.; Dye, K. M. *Environ. Impact Assess. Rev.* **2004**, *24*, 775.
(19) Clary, J. J.; Feron, V. J.; van Velthuijsen, J. A. *Regul. Toxicol. Pharmacol.* **1998**, *27*, 88.
(20) Bowner, C. T.; Hooftman, R. *Chemosphere* **1998**, *37*, 1317.
(21) Asthana, N.; Kolah, A. K.; Vu, D. R.; Lira, C. T.; Miller, D. *Org. Process Res. Dev.* **2005**, *9*, 599.
(22) Gao, J.; Zhao, X. M.; Zhou, L. Y.; Huang, Z. H. *Chem. Eng. Res. Des.* **2007**, *85*, 525.
(23) Benedict, D. J.; Parulekar, S. J.; Tsai, S. P. *Ind. Eng. Chem. Res.* **2003**, *42*, 2282.
(24) Sánchez, O.; Vidriales, G.; Morales, E.; Ortiz, E. *Chem. Eng. J.* **2006**, *117*, 123.
(25) Zhang, Y.; Yang, J. *React. Funct. Polym.* **2004**, *61*, 101.
(26) Aparicio, S.; Halajian, S.; Alcalde, R.; García, B.; Leal, J. M. *Chem. Phys. Lett.* **2008**, *454*, 49.
(27) García, B.; Aparicio, S.; Alcalde, R.; Dávila, M. J.; Leal, J. M. *Ind. Eng. Chem. Res.* **2004**, *43*, 3205.
(28) Lemmon, E. W.; McLinden, M. O.; Friend, D. G. Thermophysical Properties of Fluid Systems. In *NIST Chemistry WebBook, NIST Standard Reference Database Number 69*; Linstrom, P. J., Mallard, W. G., Eds.;

National Institute of Standards and Technology: Gaithersburg, MD, June 2005, (http://webbook.nist.gov).

(29) Ihmehls, E. C.; Gmehling, J. *Ind. Eng. Chem. Res.* **2001**, *40*, 4470.

(30) Dávila, M. J.; Aparicio, S.; Alcalde, R.; García, B.; Leal, J. M. *Green Chem.* **2007**, *9*, 221.

(31) Comuñas, M. J. P.; Baylaucq, A.; Boned, C.; Fernández, J. *Int. J. Thermophys.* **2001**, *22*, 749.

(32) Frisch, M. J.; Trucks, G. W.; Schlegel, H. B.; Scuseria, G. E.; Robb, M. A.; Cheeseman, J. R.; Montgomery, Jr., J. A.; Vreven, T.; Kudin, K. N.; Burant, J. C.; Millam, J. M.; Iyengar, S. S.; Tomasi, J.; Barone, V.; Mennucci, B.; Cossi, M.; Scalmani, G.; Rega, N.; Petersson, G. A.; Nakatsuji, H.; Hada, M.; Ehara, M.; Toyota, K.; Fukuda, R.; Hasegawa, J.; Ishida, M.; Nakajima, T.; Honda, Y.; Kitao, O.; Nakai, H.; Klene, M.; Li, X.; Knox, J. E.; Hratchian, H. P.; Cross, J. B.; Adamo, C.; Jaramillo, J.; Gomperts, R.; Stratmann, R. E.; Yazyev, O.; Austin, A. J.; Cammi, R.; Pomelli, C.; Ochterski, J. W.; Ayala, P. Y.; Morokuma, K.; Voth, G. A.; Salvador, P.; Dannenberg, J. J.; Zakrzewski, V. G.; Dapprich, S.; Daniels, A. D.; Strain, M. C.; Farkas, O.; Malick, D. K.; Rabuck, A. D.; Raghavachari, K.; Foresman, J. B.; Ortiz, J. V.; Cui, Q.; Baboul, A. G.; Clifford, S.; Cioslowski, J.; Stefanov, B. B.; Liu, G.; Liashenko, A.; Piskorz, P.; Komaromi, I.; Martin, R. L.; Fox, D. J.; Keith, T.; Al-Laham, M. A.; Peng, C. Y.; Nanayakkara, A.; Challacombe, M.; Gill, P. M. W.; Johnson, B.; Chen, W.; Wong, M. W.; Gonzalez, C.; Pople, J. A. *Gaussian 03 (Revision C.02)*; Gaussian, Inc.: Wallingford, CT, 2004.

(33) Becke, A. D. *Phys. Rev. A* **1988**, *38*, 3098.

(34) Lee, C.; Yang, W.; Parr, R. G. *Phys. Rev. B* **1988**, *37*, 785.

(35) Becke, A. D. *J. Chem. Phys.* **1993**, *98*, 5648.

(36) Cances, E.; Mennucci, B. *J. Math. Chem.* **1998**, *23*, 309.

(37) Singh, U. C.; Kollman, P. A. *J. Comput. Chem.* **1984**, *5*, 129.

(38) Besler, B. H.; Merz, K. M.; Kollman, P. A. *J. Comput. Chem.* **1990**, *11*, 431.

(39) Simon, S.; Duran, M.; Dannenberg, J. *J. Chem. Phys.* **1996**, *105*, 11024.

(40) Bader, R. F. W. *Atoms in Molecules: a Quantum Theory*; Oxford University Press, Oxford, UK, 1990.

(41) Biegler-König, F.; Schönbohm, J.; Bayles, D. *J. Comput. Chem.* **2001**, *22*, 545.

(42) Ponder, J. W. *TINKER: Software tool for molecular design 4.2*; Washington University School of Medicine: St. Louis, MO, 2004.

(43) Hoover, W. G. *Phys. Rev. A* **1985**, *31*, 1695.

(44) Allen, M. P.; Tildesley, D. J. *Computer Simulation of Liquids;* Clarendon Press: Oxford, UK, 1989.

(45) Rickaert, J. P.; Ciccotti, G.; Berendsen, H. J. *J. Comput. Phys.* **1977**, *23*, 327.

(46) Essmann, U. L.; Perera, M. L.; Berkowitz, T.; Darden, H.; Lee, H.; Pedersen, L. G. *J. Chem. Phys.* **1995**, *103*, 8577.

(47) Martínez, J. M.; Martínez, L. *J. Comput. Chem.* **2003**, *24*, 819.

(48) Jorgensen, W. L.; Maxwell, D. S.; Tirado-Rives, J. *J. Am. Chem. Soc.* **1996**, *118*, 11225.

(49) Berendsen, H. J.; Grigera, J. R.; Straatsma, T. P. *J. Phys. Chem.* **1987**, *91*, 6269.

(50) Aparicio, S.; Dávila, M. J.; Alcalde, R. *Energy Fuels* **2009**, *23*, 1591.

(51) Sanchez, I. C.; Lacombe, R. H. *Macromolecules* **1978**, *11*, 1145.

(52) Yoon, B. J. *Bull. Korean Chem. Soc.* **2003**, *24*, 1211.

(53) Dack, M. J. R. *Chem. Soc. Rev.* **1975**, *4*, 211.

(54) Sanz, M. T.; Gmehling, J. *J. Chem. Eng. Data* **2005**, *50*, 85.

(55) Fort, R. J.; Moore, W. R. *Trans. Faraday Soc.* **1966**, *62*, 1112.

(56) Cho, C. H.; Urquidi, J.; Robinson, G. W. *J. Chem. Phys.* **1999**, *111*, 10171.

(57) Cho, C. H.; Urquidi, J.; Singh, S.; Robinson, G. W. *J. Phys. Chem. B* **1999**, *103*, 1991.

(58) Miller, A. A. *J. Chem. Phys.* **1963**, *38*, 1568.

(59) Horne, R. A.; Johnson, D. S. *Phys. Chem.* **1967**, *71*, 1147.

(60) Eyring, H. *J. Chem. Phys.* **1936**, *4*, 283–291.

(61) Glasstone, S.; Eyring, H.; Laidler, K. *Theory of Rate Processes*; McGraw-Hill: New York, 1941.

(62) Aparicio, S. *J. Phys. Chem. A* **2007**, *111*, 4671.

(63) Koch, U.; Popelier, P. L. A. *J. Phys. Chem.* **1995**, *99*, 9747.

(64) Popelier, P. L. A. *J. Phys. Chem. A* **1998**, *102*, 1873.

(65) Hibbs, D. E.; Overgaard, J.; Piltz, R. O. *Org. Biomol. Chem.* **2003**, *1*, 1191.

(66) Espinosa, E.; Lecomte, C.; Molins, E. *Chem. Phys. Lett.* **1999**, *300*, 745.

(67) Espinosa, E.; Molins, E.; Lecomte, C. *Chem. Phys. Lett.* **1998**, *285*, 170.

(68) Temprado, M.; Chickos, J. S. *Thermochim. Acta* **2005**, *435*, 49.

(69) Sabbah, R.; Xu-wu, A.; Chickos, J. S.; Planas, M. L.; Roux, M. V.; Torres, L. A. *Thermochim. Acta* **1999**, *331*, 93.

(70) Kumar, R.; Schmidt, J. R.; Skinner, J. L. *J. Chem. Phys.* **2007**, *126*, 204107.

JP904668E